

Topological magnon zero-modes in dislocations

Carlos Saji¹, Nicolas Vidal-Silva², Alvaro S. Nunez¹, and Roberto E. Troncoso³

¹*Departamento de Física, FCFM, Universidad de Chile, Santiago, Chile.*

²*Departamento de Ciencias Físicas, Universidad de La Frontera, Casilla 54-D, Temuco, Chile and*

³*School of Engineering and Sciences, Universidad Adolfo Ibáñez, Santiago, Chile**

Spin fluctuations in two-dimensional (2D) ferromagnets in the presence of crystalline lattice dislocations are investigated. We show the existence of topologically protected non-propagative modes that localize at dislocations. These in-gap states, coined as *magnonic zero-modes*, are characterized by the Z_2 topological invariant that derives from parity symmetry broken induced by sublattice magnetic anisotropy. We uncover that bulk topology existing in the perfect crystal is robust under the influence of lattice defects, which is monitored by the real-space Bott index. It is also revealed that the topology of zero-modes remains unaffected when bulk topology becomes trivial and is remarkably resilient against magnetic disorder. Our findings point to the intriguing relationship between topological lattice defects and the spectrum of topological spin excitations.

Introduction.— Lattice dislocations, structural defects in ordered solids, are irregularities that emerge as abrupt changes in the crystal order. These are characterized by the Burgers vector \mathbf{B} that remains constant over the entire length of the dislocation. Dislocations in solid-state materials have been the ground for a broad range of scopes such as melting [1], elastic response, and thermal conductivity [2]. A renewed interest in dislocations promoted it to a central role in the interplay of real space topological defects and emergent band topology [3, 4]. Concretely, it was shown in topological insulators and superconductors [3, 5–17], mechanical [18–21], and light-based systems [22–25], that pair of gapless helical modes appear bound to the line defect, which are determined from the index of the dislocation modes [3],

$$N_{\text{dis}} = \frac{1}{2\pi} \mathbf{B} \cdot \mathbf{G} \pmod{2} \quad (1)$$

being the topology of these modes protected by the topological Z_2 -invariant, $\mathbf{G} = \nu_1 \mathbf{b}_1 + \nu_2 \mathbf{b}_2$, where ν_i and \mathbf{b}_i the weak topological index and reciprocal lattice vectors, respectively. Importantly, these states are robust against disorder that preserve the nontrivial bulk topology, following from the bulk-dislocation correspondence [26–28], a remarkable feature that has been experimentally demonstrated in 2D photonic crystals and metamaterials.

Quantum spin fluctuations of ordered magnets, magnons, inherit fundamental properties from the crystal lattice structure [29, 30]. It is encoded in their band spectrum and corresponding interaction with phonons, point-like defects, and structural disorder. The role of topological lattice defects on the spin-wave fluctuations has been a recurrent issue, particularly on interference and scattering effects [31–34], FMR spectra [35–37], relaxation [38, 39] and thermal conductivity [40, 41], and recently in helical textures on chiral magnets [42]. Differently, the concept of topology might emerge in the band structure of magnonic states with remarkable signatures such as robust helical edge-states and thermal Hall effect

[43, 44]. Topological magnons have been strongly scrutinized in a wide variety of spin and lattice systems [43–50], which are characterized by topological invariants that remain unchanged under smooth deformations and set the ground for the bulk-boundary correspondence [51]. The immunity of topological states to disorder, deep-rooted to topological matter [52, 53], has been tested in collinear magnets [54, 55] and glassy skyrmions [56]. However, the influence of crystal lattice defects, such as dislocations, on the band topology is an unexplored arena in magnetic systems with intriguing effects regarding the stability and localization of topological magnon states.

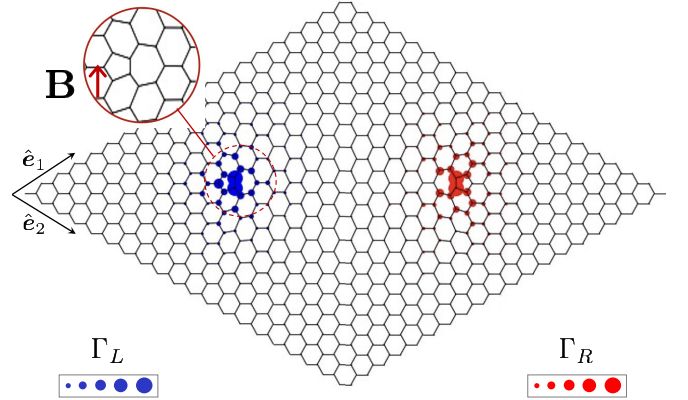


FIG. 1. Schematic representation of a pair of dislocations in the hexagonal lattice with the in-plane burgers vector $\mathbf{B} = \pm\sqrt{3}\hat{y}$, at the left and right side of the dislocations, respectively. The topological magnonic zero-modes, Γ_L (left) and Γ_R (right) states, are shown localized at the ends of the dislocation. These modes are gapped due to parity symmetry breaking, and their wave function amplitudes are, accordingly, colored differently.

In this letter, we show the existence of topological zero-dimensional magnon states bound to the dislocations (see Fig. 1) within the crystal structure of magnetic insulators. Remarkably, it is shown that magnonic zero-modes are stabilized when parity symmetry is broken and per-

sists while the topological bulk gap is closed. The existing bulk topology is diagnosed by the evaluation of a real-space topological index, the bosonic Bott index, which turns out to be stable in the presence of dislocations. It is shown that zero-modes and edge-modes have different degrees of robustness against disorder. The stability of these states is demonstrated for a model that supports a collinear ferromagnetic phase.

Spin and lattice model.— We consider a magnetic system with spins localized on a two-dimensional honeycomb lattice described by the spin Hamiltonian,

$$\mathcal{H}_S = - \sum_{\langle \mathbf{r}\mathbf{r}' \rangle} [J\mathbf{S}_{\mathbf{r}} \cdot \mathbf{S}_{\mathbf{r}'} + F(\mathbf{S}_{\mathbf{r}} \cdot \mathbf{e}_{\mathbf{r}\mathbf{r}'})(\mathbf{S}_{\mathbf{r}'} \cdot \mathbf{e}_{\mathbf{r}\mathbf{r}'}) + (K_{\mathbf{r}}(S_{\mathbf{r}}^z)^2 - BS_{\mathbf{r}}^z)\delta_{\mathbf{r}\mathbf{r}'}], \quad (2)$$

with the nearest-neighbor exchange coupling J and pseudo-dipolar interaction with strength F . The last coupling results from the spin-orbit interaction [57, 58], being $\mathbf{e}_{\mathbf{r}\mathbf{r}'}$ the unit vector that connects \mathbf{r} and \mathbf{r}' lattice sites. The easy-axis anisotropy, $K_{\mathbf{r}}$, at the $\mathcal{A}(\mathcal{B})$ -sublattice is parametrized as $K_{\mathcal{A}(\mathcal{B})} = K \pm \Delta K$, and B is the applied magnetic field along the z -direction. The dislocation is introduced following the Volterra process [59]. A set of atoms is removed, resulting in a pentagon-octagon structure, and thus, moving an equal number of steps around the dislocation sets a non-closed loop defining the Burgers vector, see Fig. 1. For numerical convenience, we consider a couple of defects that create a pair of dislocations in the bulk of the system. The local lattice deformation produces a distortion of the spin Hamiltonian, $\mathcal{H}_T = \mathcal{H}_S + \mathcal{H}_{\text{dis}}$, that gives rise to a magnetoelastic interaction \mathcal{H}_{dis} relating spin and lattice degrees of freedom.

Quantum spin fluctuations around the ordered ground state are determined by the Hamiltonian of non-interacting magnons using Holstein-Primakoff (HP) bosons [60]. Around the classical magnetic state the HP mapping of spin operators reads $S_{\mathbf{r}}^+ = (2S - a_{\mathbf{r}}^\dagger a_{\mathbf{r}})^{1/2} a_{\mathbf{r}}$, $S_{\mathbf{r}}^- = (2S - a_{\mathbf{r}}^\dagger a_{\mathbf{r}})^{1/2} a_{\mathbf{r}}^\dagger$, and $S_{\mathbf{r}}^z = S - a_{\mathbf{r}}^\dagger a_{\mathbf{r}}$. Thus, expanding the spin operators as a series in $1/S$, the spin Hamiltonian reduces to $\mathcal{H}_T \approx \mathcal{H}_0 + \mathcal{H}_m$, being \mathcal{H}_0 the classical and zero-point energy. In real space the magnon Hamiltonian reads $\mathcal{H}_m = \Psi^\dagger \mathbf{H} \Psi$, where the operator field $\Psi = (a_{\mathbf{r}}, a_{\mathbf{r}}^\dagger)^T$ with \mathbf{r} running over all lattice sites. The bosonic Hamiltonian is para-diagonalized by the Bogoliubov transformation $(a_{\mathbf{r}}, a_{\mathbf{r}}^\dagger)^T = \mathbf{T}_{\mathbf{r}\mathbf{r}'} (\alpha_{\mathbf{r}'}, \alpha_{\mathbf{r}'}^\dagger)^T$, with \mathbf{T} the paraunitary transformation that satisfy $\mathbf{T}^\dagger \zeta \mathbf{T} = \zeta$ to guarantee the commutation relation $[\alpha, \alpha^\dagger] = \mathbb{I} \otimes \sigma_z = \zeta$ for bosonic operators [61]. Therefore, the diagonalized magnon Hamiltonian is written as $\mathcal{H}_m = \sum_n \mathcal{E}_n \alpha_n^\dagger \alpha_n$ with \mathcal{E}_n the energy for the n^{th} -band.

Bulk topology.— Ferromagnetic honeycomb defects-free lattices, described by the spin Hamiltonian at Eq. (2) exhibit topological magnonic phases featured by the Chern number [50, 54, 58]. The topological gap, Δ_b , is induced

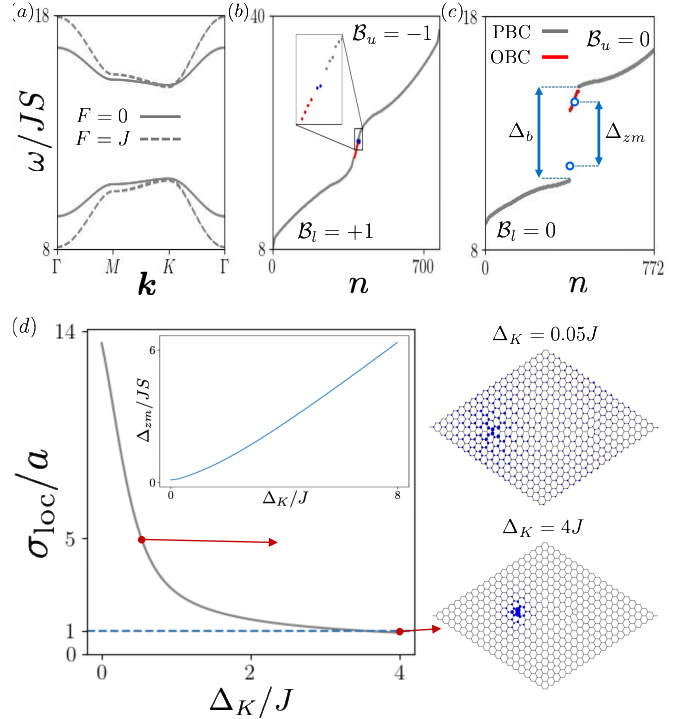


FIG. 2. (a) Bulk energy spectrum without dislocation along high-symmetry points in the Brillouin zone for $\Delta K/J = 4$, $F = 0$ (thick line), and $F = J$ (dashed line). In the presence of a dislocation, the energy spectrum with PBCs and OBCs along \hat{e}_1 direction, at (b) $K = 20J$, $\Delta K = 0$, and $F = 7J$, and (c) for $F = 0$ and $\Delta K/J = 4$. The Bott index for the lower and upper bulk bands satisfy $\mathcal{B}_u = -\mathcal{B}_l = -1$ and $\mathcal{B}_u = -\mathcal{B}_l = 0$ at panel (b) and (c), respectively. The pair of zero-magnon states, highlighted by blue dots, are gapped (Δ_{zm}) due to the sublattice anisotropy difference (Δ_K). (d) Real space localization, σ_{loc} , of magnonic zero-modes for $F = 0$, where the magnonic contribution of the zero-modes wave function $\Gamma_L(\mathbf{r})$ is depicted. At the inset, the energy gap Δ_{zm} as a function of Δ_K . All the plots are generated for the set of parameters $S = 1$ and $K/J = 8$ (except panel (b)).

by the pseudo-dipolar interaction F and controlled by the sublattice easy-axis anisotropy ΔK . We now determine the bulk topology when dislocations are present. Since crystalline symmetry is locally broken, we evaluate the topology of magnonic bands through the bosonic Bott index [54]. It is a real-space topological invariant that is equivalent to the Chern number in the thermodynamic limit and when translational invariance is restored [62–64]. For the set of eigenstates $\{\mathcal{E}_n\}$, it is defined as $\mathcal{B}(\mathcal{E}_n) = \text{Im} \left[\text{Tr} \left[\log \left(V_Y V_X V_Y^\dagger V_X^\dagger \right) \right] \right] / 2\pi$, where V_X and V_Y are unitary matrices defined by

$$P e^{i\pi\Theta} P = \mathbf{T} \zeta \begin{pmatrix} 0 & 0 \\ 0 & V_\Theta \end{pmatrix} \mathbf{T}^\dagger \zeta, \quad (3)$$

with $\Theta = X, Y$ the position operators. The projector $P = \mathbf{T} \zeta \Gamma_{\mathcal{N}} \mathbf{T}^\dagger \zeta$ on states $\{\mathcal{E}_n\}$ and the diagonal matrix $[\Gamma_{\mathcal{N}}]_{nn'} = \gamma \delta_{nn'}$, with $\gamma = 0$ for $\mathcal{N} < n$, and $\gamma = 1$

when $1 \leq n \leq \mathcal{N}$ [65]. For clean systems, the Bott index of each band is well defined and is an integer as long as $V_Y V_X V_Y^\dagger V_X^\dagger$ is nonsingular. In particular, $\mathcal{B} = 0$ when V_X and V_Y commute and the corresponding band is topologically trivial.

We now consider the effects of dislocations on the band structure and topology of magnonic states. First, in the perfect hexagonal crystal, the two-band spectrum of topologically trivial (thick line) and non-trivial (dashed line) magnon excitations is displayed in Fig. 2(a). Note that the trivial gap, induced at the Dirac point, is the result of breaking the parity symmetry by the sublattice anisotropy difference Δ_K . In the presence of dislocations, two interesting effects are highlighted from the magnonic spectrum displayed in Figs. 2(b) and (c). First, the bulk topology prevails since a non-zero Bott index is found for the top ($\mathcal{B}_u = -1$) and bottom ($\mathcal{B}_l = +1$) bands, for $F > 0$ and different dislocations lengths. In particular, the Bott index vanishes when $F = 0$ and the bulk topology becomes trivial as expected, see panel 2(c). Secondly, a pair of gapped magnonic *zero-modes* appear inside the gap, Δ_b , and bound to the ends of the dislocation, indicated by the blue dots at Fig. 2(c). The gap between these states, Δ_{zm} , is induced by non-zero values of Δ_K , which is independent of the pseudo-dipolar coupling, and therefore, becomes gapless once the parity symmetry is restored, see inset of Fig. 2(d). It is worth noting that for a strip geometry, we find that the energy of magnonic zero-modes coexist with those of topological edge-states in the presence of pseudo-dipolar energy, where open boundary conditions (OBCs) along the \hat{e}_1 axis is assumed, as is shown in Fig. 2(c).

Magnonic zero-modes are localized at the ends of the dislocation. Their spatial localization, displayed at Fig. 2, is determined from the overlap, $\Gamma_n(\mathbf{r}) = |\langle GS | a_{\mathbf{r}} \alpha_n^\dagger | GS \rangle|^2$, between the local excitation and the eigenstates, with $|GS\rangle$ the ground-state of the magnon Hamiltonian. We denote $\Gamma_{L,R}(\mathbf{r})$ to the magnonic contribution of the left- and right zero-modes wave function, displayed in Fig. 1 and 2. The magnonic zero-modes are non-propagating states, strongly bound to the lattice dislocation with localization length σ_{loc} . For a strip geometry, assuming finite size along \hat{e}_1 direction, the corresponding eigenenergies are displayed at the right of panel 2(d). In Fig. 2(d), we plot the characteristic localization length of the wave function around the dislocation as a function of Δ_K . It is defined $\sigma_{loc} = \int |\mathbf{r} - \mathbf{r}_{dis}| |\psi(\mathbf{r})|^2 d^2r$, with \mathbf{r}_{dis} the position of the dislocation and $\psi(\mathbf{r})$ the magnonic wavefunction. Interestingly, the magnonic zero-mode wave function tends to delocalize as Δ_K becomes null, corresponding to the magnonic zero-modes becoming gapless.

Weak topology and \mathbb{Z}_2 -invariant. - We now establish the topological properties of magnonic zero-modes bound to the lattice dislocations. The topology of the zero-modes

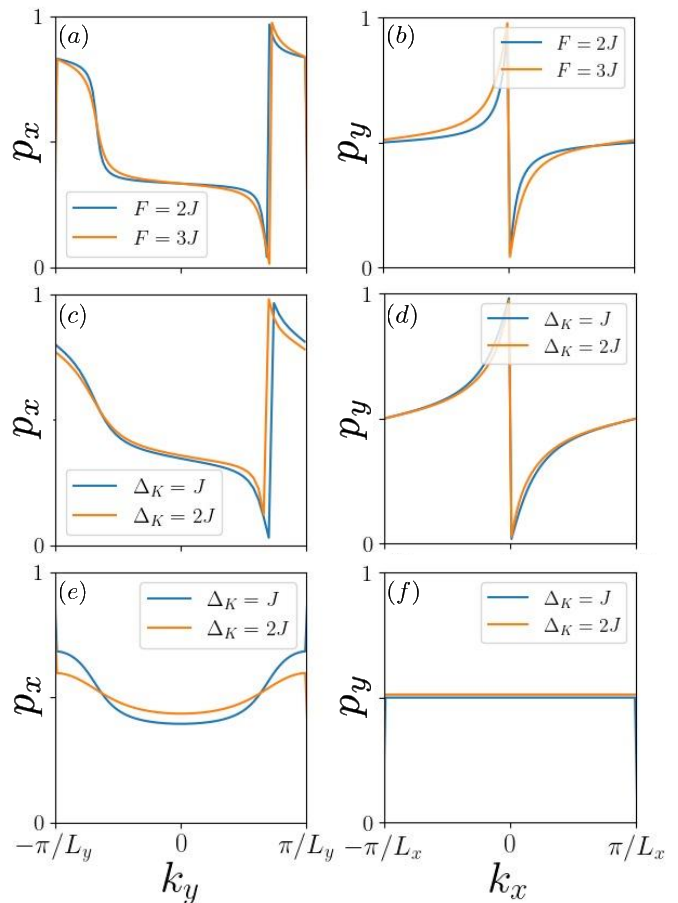


FIG. 3. Polarizations, $p_x(k_y)$ and $p_y(k_x)$, evaluated for different scenarios. At panels (a) and (b), $K = 10J$, bulk topology is nontrivial ($F > 0$), and parity symmetry is preserved ($\Delta_K = 0$). At panels (c) and (d), $K = 20J$, bulk topology is preserved ($F = 8J$) while parity symmetry is broken ($\Delta_K > 0$). In panels (e) and (f), $K = 10J$, bulk topology is trivial ($F = 0$), and parity symmetry is broken ($\Delta_K > 0$). In all plots we assumed $J = 1$.

is determined by the \mathbb{Z}_2 topological index \mathcal{G} which, through Eq. (1), determines the number of helical modes appearing at the dislocation. The \mathbb{Z}_2 -invariant and weak topological indices, ν_1 and ν_2 , are found through the bulk polarizations, defined as the sum of the Wannier centers:

$$p_x(k_y) = \sum_j \nu_x^j(k_y) \pmod{1}, \quad (4)$$

$$p_y(k_x) = \sum_j \nu_y^j(k_x) \pmod{1} \quad (5)$$

which are determined by diagonalizing the Wilson loop matrix: $W_{\mathbf{k}} | \nu_{\mathbf{k}}^j \rangle = e^{2\pi i \nu_{\mathbf{k}}^j(k_y)} | \nu_{\mathbf{k}}^j \rangle$, defined by the product

$$\mathcal{W}_{k_x} = F_{k_x + (N_x - 1)\Delta k_x, k_y} \cdots F_{k_x + \Delta k_x, k_y} F_{k_x, k_y}, \quad (6)$$

where $[F_k]^{mn} = \langle u_{k_x + \Delta k_x, k_y}^m | u_{k_x, k_y}^n \rangle_{\text{para}}$ are the overlap thought the discrete path $k_j = k_x + j\Delta k_x$. Here, we em-

ploy this formulation to compute numerically the Wannier centers $\nu_{x,y}^j$ and, therefore, the polarizations $p_x(k_y)$ and $p_y(k_x)$. In Fig. 3, we show the polarizations, $p_{x,y}$, evaluated for different scenarios. At panels (a) and (b), $K = 10J$, bulk topology is nontrivial ($F > 0$), and parity symmetry is preserved ($\Delta_K = 0$). At panels (c) and (d), $K = 20J$, bulk topology is preserved ($F = 8J$) while parity symmetry is broken ($\Delta_K > 0$). In panels (e) and (f), $K = 10J$, bulk topology is trivial ($F = 0$), and parity symmetry is broken ($\Delta_K > 0$). In all plots we assumed $J = 1$.

On the other hand, the polarization is related to the Zak phase as follows $p_\mu(k_{x,y}) = \frac{i}{2\pi} \int \sum_n \mathcal{A}_{n,\mu}(\mathbf{k}) dk_{y,x}$, where $\mathcal{A}_{n,\mu}(\mathbf{k}) = \text{Tr}[\Gamma_n \Sigma_z T_{\mathbf{k}}^\dagger \Sigma_z \partial_{k_\mu} T_{\mathbf{k}}]$ is the Berry connection and the summation runs over the lower bands (below the gap). A quantized polarization indicates that the system lies in a topological phase and provides information about high-order topological magnonic states [66]. Moreover, the weak \mathbb{Z}_2 invariants in Eq. (1) can also be computed through the Zak phase [9],

$$\nu_\mu = \frac{i}{\pi} \int_{\mathcal{C}_\mu} \sum_n \mathcal{A}_n(\mathbf{k}) \cdot d\mathbf{k}, \quad (7)$$

where the 1-cycles $\mathcal{C}_x = BZ|_{k_x=\pi/L_x}$ and $\mathcal{C}_y = BZ|_{k_y=\pi/L_y}$ run along the k_x and k_y directions in the Brillouin zone, respectively. In particular, we have that $\nu_{x,y} = 2p_{x,y}(k_{y,x} = \pi/L_{y,x})$, and according to the previous numerical calculations (see Fig. 3), we deduce that $(\nu_x, \nu_y) = (0, 1)$, and hence the \mathbb{Z}_2 -weak invariant is $\mathbf{G} = \mathbf{b}_y = \frac{2\pi}{\sqrt{3}} \hat{\mathbf{y}}$. On the other hand, the Burger vector is given by $\mathbf{B} = q(\mathbf{a}_2 - \mathbf{a}_1) = q\sqrt{3}\hat{\mathbf{y}}$, where $q = \pm 1$ is the charge of the dislocation (see Fig. 1). Finally, we arrive at $N_{\text{dis}} = \pm 1$, is non-trivial. Therefore, there must be a topologically protected dislocation mode, as we claimed.

Robustness against disorder.— Thermal fluctuations, noise, and disorder are ubiquitous and might cause negative effects on the robustness of topological properties. We now discuss the stability of existing topologically protected zero-modes at the dislocation against magnetic disorder. The disorder is modeled by a random out-of-plane magnetic field across the sample, $\mathcal{H}_{\text{random}} = \sum_i \chi S_i^z$ where $\chi \in [-\eta, \eta]$ is a random number and η is the disorder strength. Disorder-averaged magnon spectrum and magnonic zero-modes as a function of disorder strength η is depicted in Fig. 4. The results are averaged over $n = 20$ realizations of disorder in the spin lattice, where we set the anisotropy and the sublattice anisotropy difference at $K = 8J$ and $\Delta_K = 4J$, respectively. Magnonic zero-modes are remarkably robust against the effect of disordered magnetic impurities with considerable strength, resulting from topological protection. The energy of these states remains isolated within the magnon gap Δ_b , avoiding hybridization with bulk states. Although translational symmetry is broken by the presence of disorder, the localization of magnon modes at

the dislocation is not disrupted and their spatial distribution prevail.

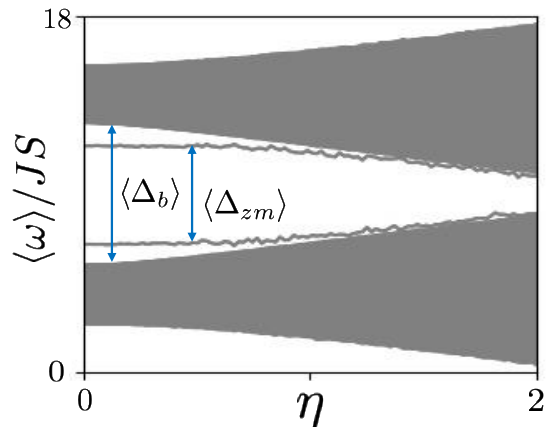


FIG. 4. The energy spectrum of magnons as a function of disorder strength η averaged over 20 realizations. Energy gaps associated with both bulk and zero-modes are depicted with vertical blue arrows.

The experimental realization of topological magnonic zero-modes might settle in two stages: first, the control of the geometrical properties of dislocations and second, on the actual excitation and local detection of different magnonic states. Advances in manufacturing and imaging techniques allow for a feasible control of dislocations density [67, 68] on the lattice, where various techniques such as XTM, STM, and AFM would enable the real-time observation of dislocations [67–71]. Magnonic zero-modes, as well as other states, can be excited by time-dependent (RF) magnetic fields, where their detection could be achieved by quantum metrology techniques [72, 73], such as nitrogen-vacancy (NV) centers, which are spin sensors that provides a local monitoring of the spatial localization of the wave function near the dislocations. Matching with the frequency of other magnonic states, would allow to detect their coexistence with topological edges-states.

Conclusions.— We have shown that bulk topology prevails in the presence of linear topological defects and dislocations in 2D hexagonal lattices. In addition, such defects induce magnonic states bound at the ends of dislocations. These states are topologically protected and classified by the \mathbb{Z}_2 -invariant, stabilized by the breaking of parity symmetry and existing even for trivial bulk topology. At the dislocation, the pair of gapped helical zero modes are determined by the relation between the Burgers vector and the topological \mathbb{Z}_2 -invariant. The presented model is general and might be employed to other forms of magnetic order.

Acknowledgments.— C.S. thanks the financial support provided by ANID National Doctoral Scholarship N°21210450. R.E.T thanks funding from Fondecyt Regu-

lar 1230747. A.S.N acknowledges funding from Fondecyt Regular 1230515. N.V-S. thanks funding from Fondecyt Iniciacion 11220046.

* roberto.troncoso.c@uai.cl

- [1] D. R. Nelson and B. I. Halperin, *Phys. Rev. B* **19**, 2457 (1979).
- [2] J. Friedel, *Dislocations*, Addison-Wesley series in metallurgy and materials (Pergamon Press; [U.S.A. ed. distributed by Addison-Wesley Publishing Company, Reading, Mass.], 1964).
- [3] Y. Ran, Y. Zhang, and A. Vishwanath, *Nature Physics* **5**, 298–303 (2009).
- [4] Z.-K. Lin, Q. Wang, Y. Liu, H. Xue, B. Zhang, Y. Chong, and J.-H. Jiang, *Nature Reviews Physics* **5**, 483–495 (2023).
- [5] J. C. Y. Teo and C. L. Kane, *Physical Review B* **82** (2010).
- [6] K.-I. Imura, Y. Takane, and A. Tanaka, *Physical Review B* **84** (2011).
- [7] D. Asahi and N. Nagaosa, *Physical Review B* **86** (2012).
- [8] A. Mesaros, Y. B. Kim, and Y. Ran, *Physical Review B* **88** (2013).
- [9] J. C. Y. Teo and T. L. Hughes, *Physical Review Letters* **111** (2013).
- [10] Z. Bi, A. Rasmussen, and C. Xu, *Physical Review B* **89** (2014).
- [11] W. A. Benalcazar, J. C. Y. Teo, and T. L. Hughes, *Physical Review B* **89** (2014).
- [12] V. Parente, G. Campagnano, D. Giuliano, A. Tagliacozzo, and F. Guinea, *Materials* **7**, 1652–1686 (2014).
- [13] R.-J. Slager, A. Mesaros, V. Juričić, and J. Zaanen, *Physical Review B* **90** (2014).
- [14] M. N. Chernodub and M. A. Zubkov, *Physical Review B* **95** (2017).
- [15] A. Panigrahi, R. Moessner, and B. Roy, *Physical Review B* **106** (2022).
- [16] F. Schindler, S. S. Tsirkin, T. Neupert, B. Andrei Bernevig, and B. J. Wieder, *Nature Communications* **13** (2022).
- [17] S. S. Yamada, T. Li, M. Lin, C. W. Peterson, T. L. Hughes, and G. Bahl, *Nature Communications* **13** (2022).
- [18] J. Paulose, B. G.-g. Chen, and V. Vitelli, *Nature Physics* **11**, 153–156 (2015).
- [19] H. Xue, D. Jia, Y. Ge, Y.-j. Guan, Q. Wang, S.-q. Yuan, H.-x. Sun, Y. Chong, and B. Zhang, *Physical Review Letters* **127** (2021).
- [20] L. Ye, C. Qiu, M. Xiao, T. Li, J. Du, M. Ke, and Z. Liu, *Nature Communications* **13** (2022).
- [21] Y. Deng, W. A. Benalcazar, Z.-G. Chen, M. Oudich, G. Ma, and Y. Jing, *Physical Review Letters* **128** (2022).
- [22] F.-F. Li, H.-X. Wang, Z. Xiong, Q. Lou, P. Chen, R.-X. Wu, Y. Poo, J.-H. Jiang, and S. John, *Nature Communications* **9** (2018).
- [23] J. Lu, K. G. Wirth, W. Gao, A. Heßler, B. Sain, T. Taubner, and T. Zentgraf, *Science Advances* **7** (2021).
- [24] B.-Y. Xie, O. You, and S. Zhang, *Physical Review A* **106** (2022).
- [25] A. Agarwala and V. B. Shenoy, *Phys. Rev. Lett.* **118**, 236402 (2017).
- [26] M. Geier, I. C. Fulga, and A. Lau, *SciPost Physics* **10** (2021).
- [27] Y. Liu, S. Leung, F.-F. Li, Z.-K. Lin, X. Tao, Y. Poo, and J.-H. Jiang, *Nature* **589**, 381–385 (2021).
- [28] Y. Kubota, *Journal of Physics A: Mathematical and Theoretical* **54**, 364001 (2021).
- [29] W. Brinkman, *J. Appl. Phys.* **38**, 939–943 (1967).
- [30] R. Birss, *Symmetry and Magnetism*, Series of monographs on selected topics in solid state physics No. v. 3 (North-Holland Publishing Company, 1964).
- [31] V. L. Pokrovskii, *ZhETF Pisma Redaktsiui* **11**, 233 (1970).
- [32] A. N. Kuchko and M. V. Chernyshëva, *Physics of the Solid State* **40**, 1861–1863 (1998).
- [33] L. A. Turski and M. Mińkowski, *Journal of Physics: Condensed Matter* **21**, 376001 (2009).
- [34] S. G. Gestrin and E. A. Sal’nikova, *Russian Physics Journal* **54**, 1177–1184 (2012).
- [35] V. Bar’yakhtar, M. Savchenko, and V. Tarasenko, *Journal of Experimental and Theoretical Physics* **27**, 858 (1968).
- [36] J. Zmijan and J. Spalak, *Solid State Communications* **35**, 699–703 (1980).
- [37] M. Schmidt, *Le Journal de Physique Colloques* **49**, C8 (1988).
- [38] J. Morkowski, *Physics Letters A* **26**, 144–145 (1968).
- [39] J. Morkowski, *Journal de Physique Lettres* **35**, 257–259 (1974).
- [40] V. Bar’yakhtar, M. Savchenko, and V. Tarasenko, *Journal of Experimental and Theoretical Physics* **24**, 623 (1967).
- [41] A. Fomethé and G. Maugin, *International Journal of Engineering Science* **20**, 1125–1144 (1982).
- [42] M. Azhar, V. P. Kravchuk, and M. Garst, *Phys. Rev. Lett.* **128**, 157204 (2022).
- [43] Z.-X. Li, Y. Cao, and P. Yan, *Physics Reports* **915**, 1–64 (2021).
- [44] F. Zhuo, J. Kang, A. Manchon, and Z. Cheng, *Advanced Physics Research* (2023).
- [45] Y. Onose, T. Ideue, H. Katsura, Y. Shiomi, N. Nagaosa, and Y. Tokura, *Science* **329**, 297 (2010).
- [46] L. Zhang, J. Ren, J.-S. Wang, and B. Li, *Phys. Rev. B* **87**, 144101 (2013).
- [47] A. Mook, J. Henk, and I. Mertig, *Phys. Rev. B* **90**, 024412 (2014).
- [48] S. K. Kim, H. Ochoa, R. Zarzuela, and Y. Tserkovnyak, *Phys. Rev. Lett.* **117**, 227201 (2016).
- [49] R. Shindou, R. Matsumoto, S. Murakami, and J.-i. Ohe, *Phys. Rev. B* **87**, 174427 (2013).
- [50] X. S. Wang and X. R. Wang, *Journal of Applied Physics* **129** (2021).
- [51] B. A. Bernevig and T. L. Hughes, *Topological Insulators and Topological Superconductors* (STU-Student edition. Princeton University Press., 2013).
- [52] M. Z. Hasan and C. L. Kane, *Rev. Mod. Phys.* **82**, 3045 (2010).
- [53] X.-L. Qi and S.-C. Zhang, *Rev. Mod. Phys.* **83**, 1057 (2011).
- [54] X. S. Wang, A. Brataas, and R. E. Troncoso, *Phys. Rev. Lett.* **125**, 217202 (2020).
- [55] Y. Akagi, *Journal of the Physical Society of Japan* **89**, 123601 (2020).
- [56] H. D. Rosales and R. E. Troncoso, “Robustness of

- topological magnons in disordered arrays of skyrmions,” (2024), [arXiv:2404.06541](https://arxiv.org/abs/2404.06541) [[cond-mat.mes-hall](https://arxiv.org/abs/2404.06541)].
- [57] G. Jackeli and G. Khaliullin, *Phys. Rev. Lett.* **102**, 017205 (2009).
- [58] X. S. Wang, Y. Su, and X. R. Wang, *Phys. Rev. B* **95**, 014435 (2017).
- [59] H. Kleinert, *Gauge Fields in Condensed Matter* (WORLD SCIENTIFIC, 1989).
- [60] T. Holstein and H. Primakoff, *Phys. Rev.* **58**, 1098 (1940).
- [61] J. Colpa, *Phys. A: Stat. Mech. Appl.* **93**, 327 (1978).
- [62] T. A. Loring and M. B. Hastings, *EPL (Europhysics Letters)* **92**, 67004 (2010).
- [63] D. Toniolo, *Phys. Rev. B* **98**, 235425 (2018).
- [64] D. Toniolo, *Letters in Mathematical Physics* **112** (2022), [10.1007/s11005-022-01602-6](https://doi.org/10.1007/s11005-022-01602-6).
- [65] For fermionic systems the metric $\eta = \mathbb{I}$ and the definition in the main text returns to the electronic Bott index.
- [66] Z. Li, Y. Cao, P. Yan, and X. Wang, *npj Computational Materials* **5** (2019), [10.1038/s41524-019-0246-4](https://doi.org/10.1038/s41524-019-0246-4).
- [67] H. Zheng, Y. S. Meng, and Y. Zhu, *Mrs Bulletin* **40**, 12 (2015).
- [68] Q. Yu, M. Legros, and A. Minor, *Mrs Bulletin* **40**, 62 (2015).
- [69] P. G. Callahan, B. B. Haidet, D. Jung, G. G. Seward, and K. Mukherjee, *Physical Review Materials* **2**, 081601 (2018).
- [70] O. Schaff, A. K. Schmid, N. C. Bartelt, J. de la Figuera, and R. Q. Hwang, *Materials Science and Engineering: A* **319**, 914 (2001).
- [71] T. Tsuji and K. Yamanaka, *Nanotechnology* **12**, 301 (2001).
- [72] P. Andrich, C. F. de las Casas, X. Liu, H. L. Bretscher, J. R. Berman, F. J. Heremans, P. F. Nealey, and D. D. Awschalom, *npj Quantum Information* **3**, 28 (2017).
- [73] C. Purser, V. Bhallamudi, F. Guo, M. Page, Q. Guo, G. Fuchs, and P. Hammel, *Applied Physics Letters* **116** (2020), <https://doi.org/10.1063/1.5141921>.